HOKKAIDO UNIVERSITY

Title	Detection of ambrosia beetles using a pan-sharpened image generated from ALOS/AVNIR-2 and ALOS/PRISM imagery
Author(s)	Sonobe, Rei; Tani, HIroshi; Wang, Xiufeng
Citation	Forest Systems, 23(1), 178-182 https://doi.org/10.5424/fs/2014231-04572
Issue Date	2014
Doc URL	https://hdl.handle.net/2115/54962
Type	journal article
File Information	Detection of ambrosia beetles using ALOS.pdf



Hokkaido University Collection of Scholarly and Academic Papers : HUSCAP

Instituto Nacional de Investigación y Tecnología Agraria y Alimentaria (INIA)
Available online at www.inia.es/forestsystems
http://dx.doi.org/10.5424/fs/2014231-04572

Forest Systems 2014 23(1): 178-182
ISSN: 2171-5068
eISSN: 2171-9845

Short communication. Detection of ambrosia beetles using a pan-sharpened image generated from ALOS/AVNIR-2 and ALOS/PRISM imagery

Rei Sonobe[1]*, Hiroshi Tani[2] and Xiufeng Wang[2]

[1] Graduate School of Agriculture. Hokkaido University. Kita 9. Nishi 9 Kita-ku. Sapporo, Japan. [2] Research Faculty of Agriculture. Hokkaido University. Kita 9. Nishi 9 Kita-ku. Sapporo, Japan

Abstract

Aim of study: The ambrosia beetle, *Platypus quercivorus*, is a vector of Japanese oak wilt, which causes massive mortality of oak trees in Japan. ALOS/AVNIR-2 true color images can be used to help detect areas of oak wilt, although such detection by inventory surveys is not realistic. Applying pan-sharpening techniques, a higher spatial resolution multispectral image can be generated from lower-resolution multispectral images and higher-resolution panchromatic images. In this study, some pan-sharpening algorithms were considered and evaluated for the detection of damage points.

Area of study: The oak forests in Kanazawa prefecture, Japan.

Material and methods: The ALOS/AVNIR-2 and ALOS/PRISM sensors were used. The pan-sharpening algorithms adopted were: Brovey transformation, Modified IHS transformation, Wavelet transformation, Ehlers fusion and High Pass Filter Resolution Merge. Four types of quantitative spectral analyses and visual detection were conducted to evaluate these algorithms.

Main results: The Brovey transformation was the most useful algorithm to detect damage points, although it had an issue with the preservation of spectral characteristics.

Research highlights: The detection rate of damage points was improved in 50% by applying the Brovey algorithm to a 10 m panchromatic image and 62.5 m multispectral image.

Key words: ambrosia beetle; oak wilt; pan-sharpening; satellite imagery; visual detection.

Introduction

Since the late 1980s, deciduous oak dieback has been prevalent in Japan, but recently, the infestation has lasted, and the area of dieback has spread to new localities where diebacks have never been recorded (Ito and Yamada, 1998). The major vector of this fungus is the ambrosia beetle, *Platypus quercivorus* (Murayama), is a major vector of this fungus. Ambrosia beetles are wood-inhabiting, obligate mutualistic insects that construct galleries within which they cultivate fungi for food (Hulcr *et al.*, 2007) and usually attack weakened or dead trees; *e.g.,* the southern pine beetle (Rojas *et al.*, 2010), the european elm bark beetle (Hubbes, 2004) and the spruce beetle (Makoto *et al.*, 2013). Since ambrosia fungus cause the problems of oak wilt, decrease of wood resources and galleries, the determining the pattern of insect presence is a matter of great urgency.

* Corresponding author: reysnb@env.agr.hokudai.ac.jp
Received: 04-06-13. Accepted: 05-09-13.

There are many studies of forest monitoring using satellite remote sensing (Cano *et al.*, 2005; Blanco *et al.*, 2009), and in this case, detecting points of insect presence using an ALOS/AVNIR-2 true color image will be useful (Kamibayashi *et al.*, 2008). Furthermore, applying pan-sharpening technics, higher spatial resolution multispectral image can be generated from a combination of lower resolution multispectral images and higher resolution panchromatic images.

A great number of pan-sharpening techniques have been developed to combine panchromatic and multispectral images to produce an enhanced multispectral image with a high spatial resolution. Currently, simple pan-sharpening algorithms, such as the Brovey transformation, are widely used (Ehlers *et al.*, 2010). Over the last few years, a number of improved algorithms have been developed with the promise to minimize color distortion while retaining the spatial improvement. In this study, five pan-sharpening algorithms were chosen for comparison. These algorithms include the modified IHS transformation (IHS),

Wavelet transformation (Wavelet) Ehlers fusion (Ehlers) and High Pass Filter Resolution Merge (HPF). For comparison, we also selected the Brovey transformation (Brovey).

The difference in spatial resolution between the panchromatic and multispectral modes can be measured by the resolution ratio (RR), and an RR between 1:2 and 1:5 is generally adopted (Madden, 2009). Thus, for the detection of damage points, the effects of the RR were evaluated, and some pan-sharpening algorithms were considered and evaluated.

Material and methods

The study area were oak forests composed of *Quercus crispula* Blume and *Quercus serrata* Murray in Kanazawa prefecture, Japan. The forests were suffering from problem of oak wilt, culturing mushrooms, decrease of wood resources and galleries caused by the ambrosia beetle.

The satellite data were acquired on September 11, 2007 by ALOS/PRISM and AVNIR-2 (Table 1). First, the PRISM imagery was resampled with a 10 m pixel resolution (equal to the original AVNIR-2 imagery). Second, the AVNIR-2 imagery was resampled with resolutions of 20, 30, 40, 50 and 62.5 m (to simulate the RR of ALOS-3/HISUI, which would be launched in 2014) because an RR between 1:2 and 1:5 is generally desirable. Third, pan-sharpened imagery was generated with a pixel spacing of 10 m, and then the original AVNIR-2 imagery was compared to evaluate the preservation of the spectral characteristics by the pan-sharpening algorithms. In this study, five pan-sharpening algorithms (IHS, Wavelet, Ehlers, HPF and Brovey) were chosen for comparison. The IHS transform separates spatial (intensity) and spectral (hue and saturation) information from a standard RGB image. To fuse the images, three bands of a multispectral image are transformed from the RGB domain into the IHS color space. We make use of the modified IHS fusion from Siddiqui (2003) which was developed for a better fit of the fused multispectral bands to the original data. Wavelet transformation is based on the wavelet decomposition of images into different components based on their local frequency content. We perform the Discrete Wavelet Transforms (DWT) on the multispectral and panchromatic images to extract the low frequency data from the multispectral image and the high frequency data from the panchromatic image. These components are combined to create the Fused Wavelet Coefficient Map. The inverse wavelet transformation is performed on the fused map to create the final pan-sharpened image. The Ehlers fusion is based on an IHS transform coupled with a Fourier domain filtering. This technique is extended to include more than 3 bands by using multiple IHS transforms until the number of bands is exhausted. A subsequent Fourier transform of the intensity component and the panchromatic image allows an adaptive filter design in the frequency domain. Using fast Fourier transform (FFT) techniques, the spatial components to be enhanced or suppressed can be directly accessed. The intensity spectrum is filtered with a low pass filter (LP) whereas the panchromatic spectrum is filtered with an inverse high pass filter (HP). After filtering, the images are transformed back into the spatial domain with an inverse FFT and added together to form a fused intensity component with the low-frequency information from the low resolution multispectral image and the high-frequency information from the high resolution image. This new intensity component and the original hue and saturation components of the multispectral image form a new IHS image. As the last step, an inverse IHS transformation produces a fused RGB image. These steps can be repeated with successive 3-band selections until all bands are fused with the panchromatic image (Ehlers, 2004). The algorithm shows the best result for the preservation of spectral characteristics (Ehlers *et al.*, 2010). Then we thought this algorithm would be the most useful algorithm for visually analysis. HPF is an arithmetic technique that applies a spatial enhancement filter to the high-resolution image before being merged with the multispectral data set on a pixel-by-pixel basis. The HPF combines both spatial and spectral information using the band addition approach (Chávez *et al.*, 1991). Brovey uses a ratio algorithm to combine the multispectral and panchromatic images. Essentially the technique normalizes each of the multispectral bands used and multiplies these with the higher resolution panchromatic band. When layer stacked, the result is a synthesized higher resolution multispectral image (Pohl and Van Genderen, 1998).

Table 1. Characteristics of the satellite images used

Sensor	Date	Incidence angle (°)	Pixel spacing (m)
ALOS/PRISM	September 11,	–1.2	2.5
ALOS/AVNIR-2	2007	0	10

Four statistical measures were used for the quantitative spectral evaluation. The correlation coefficient (CC) between the original multispectral bands and the equivalent fused bands was calculated to evaluate the spectral value preservation. The values ranged from –1 to 1, and good correspondence is close to 1. For the per-pixel deviation (PD) (Wald 2002), the fused image was first degraded to the spatial resolution of the original image and was then subtracted from the original image on a per-pixel basis. Then, the average deviation per pixel was calculated using the number of pixels in the image. Desirable low differences between the original and fused images were indicated by low values of the PD, with minimum of 0. The root mean square error (RMSE) was also proposed by Wald (2002), and its best possible value is 0. The structure similarity index (SSIM) combined comparisons of luminance, contrast and structure (Wang *et al.*, 2004). The values range between 0 and 1, and values close to 1 showed the highest correspondence with the original images.

As a qualitative evaluation, visual detection was conducted. Using visual detection, the detection rate of the points of oak wilt was evaluated for the AVNIR-2 imagery (original and resampled imagery) and the pan-sharpened imagery.

Results and discussion

Using a spectrometer (ASD Inc. FieldSpec 3), the reflection characteristics of the normal leaves and the damaged leaves are shown in Fig. 1, and the differences were observed in the three bands of AVNIR-2. Thus, the points of oak wilt can be detected visually using AVNIR-2 true color imagery (red: 610-690 nm, green: 520-600 nm and blue: 420-500 nm).

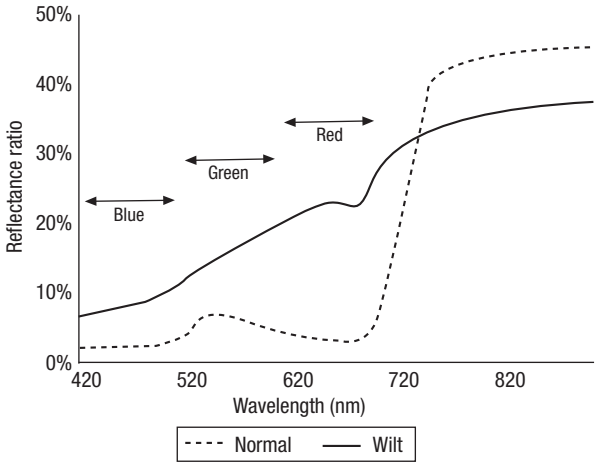


Figure 1. Reflectance ratios of the leaves and wavelengths of ALOS/AVNIR-2 (red, green and blue).

The results of the quantitative and qualitative evaluations are shown in Table 2.

Better CC's were obtained by the HPF (average of 0.82), Brovey and Ehlers (averages of 0.74) and the difference between HPS and Brovey is significant at 5% level ($p = 0.017$). For the blue band, in particular IHS, the CC's were lower than for the other two bands ($p > 0.01$) because the range of the original blue band is not completely covered by the PRISM sensor (520-770 nm). For the red and green bands, the Wavelet has the worst result (the differences were significant at 1% level), whereas the four other algorithms had CC's that were greater than 0.7 for all pixel spacings. In general, the Wavelet was strongly subject to the influence of the degradation caused by resampling (Ehlers *et al.*, 2010).

Ehlers *et al.* (2010) shows that the PD less than 5.0 means acceptable. For the HPF, IHS and Wavelet, the PDs were less than 5.0, indicating that good results were obtained. However, the worst PDs were obtained by the Brovey, in agreement with other studies, in which, the results of the Ehlers were not associated with the pixel spacing (Ehlers *et al.*, 2010).

The best RMSEs were obtained for the HPF, whereas the worst results were obtained for the Brovey [the RMSEs for Brovey were 20-55 worse than those for HPF and the difference were significant at 1% level ($p < 0.01$)]. Compared with the other algorithms, the Ehlers was strongly subject to the influence of the degradation caused by resampling. The capacity of edge detection of pan-sharpened image applying Ehlers algorithm is relatively low (Ehlers *et al.*, 2010). The algorithm was weak against the ambiguity of multispectral image by the degradation. Again, the best SSIMs were observed for the HPF, and the worst results were obtained for the Brovey.

The visual detection of the original AVNIR-2 imagery enabled the extraction of 1,044 damage points. The detection rate of the damage points was 78.0%, 70.4%, 48.9%, 48.5% and 38.2% for pixel spacings of 20 m, 30 m, 40 m, 50 m and 62.5 m, respectively. Additionally, color compensations were conducted for all pan-sharpened imagery to support visual detection. In the case of an RR of 1:6.25, all algorithms were useful for the visual detection. In particular, the Brovey was the most effective algorithm for edge detection and as a consequence, the detection rate of damage

Table 2. Quantitative and qualitative evaluations. The numbers separated with commas are the results for red, green and blue, respectively. The abbreviations Brovey, HPF, Ehlers, IHS and Wavelet are the Brovey transformation, High Pass Filter Resolution Merge, Ehlers fusion, the modified IHS transformation and Wavelet transformation, respectively

Algorithm	Pixel spacing (m)	Quantitative spectral analysis				Qualitative evaluation
		Correlation coefficient (CC)	Per-pixel derivation (PD)	Root mean square error (RMSE)	Structure similarity index (SSIM)	Detection rate
Brovey	20	0.89, 0.80, 0.64	26.18, 41.10, 58.42	27.53, 41.94, 58.60	0.23, 0.22, 0.25	88,7%
	30	0.87, 0.79, 0.60	26.21, 41.03, 58.27	27.54, 41.95, 58.61	0.22, 0.22, 0.25	78,9%
	40	0.83, 0.77, 0.60	26.22, 41.09, 58.34	27.61, 41.96, 58.61	0.21, 0.22, 0.25	74,8%
	50	0.83, 0.77, 0.60	26.12, 41.06, 58.30	27.66, 41.96, 58.65	0.21, 0.22, 0.25	71,0%
	62.5	0.79, 0.76, 0.60	26.24, 41.06, 58.31	27.70, 41.99, 58.69	0.20, 0.22, 0.25	59,2%
HPF	20	0.89, 0.89, 0.88	0.36, 0.28, 0.26	5.40, 5.09, 3.52	0.89, 0.89, 0.87	85,0%
	30	0.85, 0.83, 0.84	0.39, 0.31, 0.29	6.23, 6.21, 3.96	0.85, 0.83, 0.83	67,0%
	40	0.82, 0.83, 0.81	0.34, 0.25, 0.23	6.64, 6.28, 4.20	0.83, 0.83, 0.81	64,9%
	50	0.82, 0.81, 0.80	0.39, 0.32, 0.28	6.75, 6.61, 4.29	0.82, 0.81, 0.79	61,2%
	62.5	0.74, 0.71, 0.73	0.40, 0.32, 0.29	8.04, 8.01, 4.96	0.75, 0.72, 0.73	52,7%
Ehlers	20	0.90, 0.84, 0.66	1.71, 24.51, 6.86	5.36, 7.02, 6.90	0.89, 0.76, 0.66	89,3%
	30	0.88, 0.81, 0.63	0.52, 1.00, 21.63	5.50, 7.73, 9.73	0.88, 0.79, 0.64	69,7%
	40	0.83, 0.79, 0.63	0.54, 13.30, 0.20	6.26, 14.96, 12.72	0.84, 0.75, 0.63	47,3%
	50	0.84, 0.77, 0.58	0.84, 12.97, 11.92	6.35, 14.97, 14.17	0.84, 0.75, 0.58	45,5%
	62.5	0.78, 0.74, 0.55	6.70, 0.76, 10.55	10.13, 25.36, 23.23	0.77, 0.71, 0.52	42,7%
IHS	20	0.90, 0.80, 0.54	0.45, 0.48, 0.31	5.02, 6.81, 8.53	0.90, 0.80, 0.52	62,2%
	30	0.88, 0.80, 0.52	0.46, 0.53, 0.42	5.56, 6.87, 8.80	0.86, 0.80, 0.52	58,1%
	40	0.85, 0.71, 0.43	0.57, 0.52, 0.31	6.00, 7.79, 8.93	0.84, 0.72, 0.46	49,1%
	50	0.84, 0.71, 0.38	0.37, 0.37, 0.29	6.35, 7.83, 9.14	0.81, 0.71, 0.41	42,3%
	62.5	0.81, 0.71, 0.35	0.42, 0.35, 0.26	6.77, 7.97, 9.59	0.78, 0.71, 0.37	20,3%
Wavelet	20	0.77, 0.77, 0.71	0.06, 0.17, 0.14	7.68, 7.51, 5.80	0.78, 0.77, 0.73	72,0%
	30	0.74, 0.73, 0.70	0.09, 0.19, 0.22	8.28, 8.11, 5.81	0.74, 0.74, 0.72	64,8%
	40	0.60, 0.60, 0.55	0.25, 0.27, 0.24	10.12, 9.95, 7.42	0.61, 0.61, 0.57	56,5%
	50	0.53, 0.54, 0.51	0.14, 0.25, 0.25	11.01, 10.67, 7.64	0.55, 0.55, 0.54	51,4%
	62.5	0.44, 0.45, 0.41	0.36, 0.50, 0.63	12.08, 11.82, 9.30	0.46, 0.46, 0.42	47,3%

points improved by 50%. Then, the Brovey had the best results for the RRs of 1:3, 1:4 and 1:5, and the Ehlers was the most useful for an RR of 1:2. These results were similar to those of the CC.

Conclusions

With respect to the quantitative spectral analysis evaluations, HPF had good results and thus may be potentially applied to various remote sensing techniques, such as unsupervised classification and NDVI calculations. In contrast, Brovey had the worst results except for the correlation coefficients, which showed that the detection rate of the damage point was high. These results indicated that the degradation of the spectral characteristics can be overcome, even if the correlation coefficients between the original multispectral imagery and the pan-sharpened imagery are high, in the case for which the primary aim is to detect damage points. Then this algorithm may be used widely for detecting insect distribution using the satellites launched in future such as ALOS-3.

Acknowledgements

Our research was supported financially by the Hokkaido Intellect Tank (HIT). For the in-situ survey, we received great help from Mr. Norihisa Kamibayashi of Remote Sensing Technology Center of Japan (RESTEC) and Dr. Naoto Kamata of the University of Tokyo.

Finally, many thanks to Dr. Rafael Calama and all reviewers for their helpful comments.

References

Blanco E, Bonet JA, Eizaguirre M, 2009. Using Landsat satellite imagery to detect small-size forest stands of *Pinus nigra* Arn. and *Pinus sylvestris* L. affected by Scolytidae. For Syst 18: 264-275.

Cano F, Cerrillo RMN, Ferrer AG, Orden MS, 2005. Forest defoliation using IKONOS sensor for cork oak (*Quercus suber* L.) woods in Southern Spain. For Syst 14: 242-252.

Chavez PS, Sildes SC, Anderson JA, 1991. Comparison of three different methods to merge multiresolution and multispectral data: landsat TM and SPOT panchromatic. Photogramm Eng Remote Sen. 57: 295-303.

Ehlers M, 2004. Spectral characteristics preserving image fusion based on Fourier domain filtering. Proc SPIE, Maspalomas, Spain, 5574. pp: 1-13.

Ehlers M, Klonus S, Åstrand PJ, Rosso P, 2010. Multi-sensor image fusion for pansharpening in remote sensing, Int J Image Data Fusion 1: 25-45.

Hubbes M, 2004. Induced resistance for the control of Dutch elm disease. For Syst 13: 185-196.

Hulcr J, Mogia M, Isua B, Novotny V, 2007. Host specificity of ambrosia and bark beetles (Col., Curculionidae: Scolytinae and Platypodinae) in a New Guinea rain forest. Ecol Entomol 32: 762-772.

Ito S, Yamada T, 1998. Distribution and spread of mass mortality of oak trees. J Jpn For Soc 80: 229-232.

Kamibayashi N, Tani H, Kamata N, 2008. Detection of insect damage using ALOS/AVNIR-2. Proc JSPRS Annu Conf. pp: 131-132.

Madden M, 2009. Manual of Geographic Information Systems. American society for Photogrammetry and Remote Sensing, Bethesda. 1352 pp.

Makoto K, Tani H, Kamata N, 2013. High-resolution multispectral satellite image and a postfire ground survey reveal prefire beetle damage on snags in Southern Alaska, Southern Alaska. Scand J For Res.

Pohl C, Van Genderen JL, 1998. Multisensor image fusion in remote sensing: concepts, methods and applications. Int J Remote Sens 19: 823-854.

Rojas MR, Locatelli B, Billings R, 2010. Climate change and outbreaks of Southern Pine Beetle in Honduras. For Syst 19: 70-76.

Siddiqui Y, 2003. The modified IHS method for fusing satellite imagery, Proc 2003 ASPRS Annual Convention, Anchorage, 10.

Wald L, 2002. Data fusion: definitions and architectures – fusion of images of different spatial resolutions. Presses des MINES, Paris. 198 pp.

Wang Z, Bovik AC, Sheikh HR, Simoncelli EP, 2004. Image quality assessment: from error visibility to struct1ural similarity. IEEE Trans Image Process 13: 600-612.1.